Detailed studies of mid-ocean ridge volcanism at the Mid-Atlantic Ridge (45N) and elsewhere

YEO, ISOBEL,ALICE,L

Geology

Eruptive hummocks: Building blocks of the upper ocean crust

Isobel Yeo, Roger C. Searle, Kay L. Achenbach, Tim P. Le Bas and Bramley J. Murton

Geology 2012;40;91-94
doi: 10.1130/G31892.1

Notes

Eruptive hummocks: Building blocks of the upper ocean crust

Isobel Yeo[1]*, Roger C. Searle[1], Kay L. Achenbach[1], Tim P. Le Bas[2], and Bramley J. Murton[2]
[1]Department of Earth Sciences, Durham University, Durham, DH1 3LE, UK
[2]National Oceanography Centre, Empress Dock, Southampton SO14 3ZH, UK

ABSTRACT

The spreading axis at many slow-spreading mid-ocean ridges is marked by an axial volcanic ridge. In this study, we use a combination of high-resolution remote sensing methods to elucidate the detailed nature of volcanoes in such a ridge. We find that the "hummocks" described in previous sidescan sonar studies are dome- or cone-shaped edifices, 5–150 m high with diameters of 30–330 m. We estimate they form quickly, in single eruptions, each of which may produce several hummocks. Hummock collapse is common and hummocks of all heights are prone to failure. Collapses generally occur down the regional seafloor slope, suggesting control by local topography. Approximately 33% of hummocks lose ~40% of their volume by collapse, so ~12% of all material erupted on the axial volcanic ridge is rapidly converted to talus. The higher porosity of these deposits may increase average upper crustal porosity by several percent, contributing >0.5 km s^{-1} to seismic velocity decrease in the upper oceanic crust, and may be one of the dominant mechanisms for increasing porosity in upper slow-spreading oceanic crust.

INTRODUCTION

Most slow-spreading mid-ocean ridge segments contain an axial volcanic ridge (AVR). AVRs are composite volcanoes composed of successive units of erupted basalts that build on each other to produce a topographic high (Ballard and Moore, 1977; Smith and Cann, 1993). They are thought to be the focus of volcanism at slow-spreading ridges and thus the location for the production of upper oceanic crust (Smith and Cann, 1992, 1993). In this paper, we examine an AVR at the scale of individual eruptions in order to understand the physical processes and time scales that characterize this fundamental feature of slow-spreading ridges.

Eruptions that make up the AVR build hummocks, described as "rounded mounds 50–500 m in diameter with relief <50 m" (Smith and Cann, 1990, p. 712). While they have been described by a combination of sidescan sonar, photographs, and submersible observations in the past, previous multibeam mapping was not sufficient to resolve them. In this study, we use new high-resolution multibeam data alongside sidescan sonar and remotely operated vehicle (ROV) observations to provide a three-dimensional (3-D) perspective.

We confirm that individual sidescan hummocks are small, probably monogenetic, volcanic edifices. We define their geometry, estimate their eruption times, and assess their relationship to each other and to the AVR. We also identify numerous collapse scarps, and discuss their formation and implications for seismic layer 2A.

STUDY AREAS AND DATA ACQUISITION

This study focuses on the Mid-Atlantic Ridge (MAR) at 45°N (Fig. 1), a typical MAR spreading segment, containing a 22-km-long, 600-m-high AVR (Fig. 1). Two sites were chosen for detailed study. Area 1 (Figs. 1 and 2) is on the eastern flank of the magmatically robust southern part of the AVR (Searle et al., 2010). It covers ~5 km^2 from the AVR crest to its base at the eastern axial valley wall. Area 2 (see the GSA Data Repository[1]) provides an almost complete (~5.7 km) oblique transect across the lower-lying, probably older, AVR, north of 45°32′N.

Sidescan sonar (30 kHz) was acquired using the deep-towed TOBI system (towed ocean bottom instrument; Flewellen et al., 1993), and microbathymetry and seafloor video from the ROV *Isis* (German et al., 2003), both operated by the National Oceanography Centre (Southampton, UK).

TOBI's sidescan sonar covers a 6 km swath with a pixel size of 3 m, and estimated post-processed navigational precision of ~100 m (LeBas and Huvenne, 2009). 1.5-km-spaced east-west tracks yielded complete north- and south-looking sidescan coverage of the entire axial valley (Searle et al., 2010).

ROV *Isis* carried video and high-resolution still cameras and, for one dive in each detailed study area, a Simrad SM2000 bathymetry system, yielding bathymetry with a horizontal and vertical resolution of ~1–2 m. Area 1 also had >17 km of continuous near-bottom visual observations from three dives (Fig. 2).

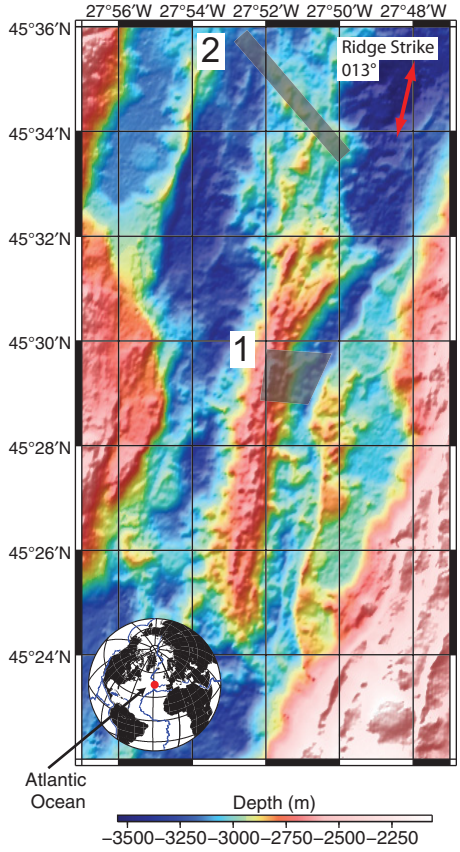

Figure 1. Location map and shipboard EM120 bathymetry of Mid-Atlantic Ridge at 45°N (location inset). Prominent 22-km-long axial volcanic ridge (AVR) extends from 45°24′N to 45°36′N within the axial valley. Arrows show spreading direction (097.9°). High-resolution study areas 1 and 2 are highlighted in gray. Most recently active AVR is shown by the area shallower than 2900 m (yellow and red). A presumed older, more-tectonized AVR (Searle et al., 2010) extends north of 45°32′N (shallower than 3100 m, pale blue). Entire area shown is covered by sidescan sonar.

OBSERVATIONS

We identified nearly 3000 hummocks on the AVR surface from sidescan sonar, with diameters of 5–450 m; 153 were imaged in high-resolution study areas 1 and 2. There is a one-to-one correspondence between sidescan hummocks and conical or domed volcanic edifices in the SM2000 bathymetry (Fig. 2). Similar to Smith and Cann (1990), we identified hummocks from the high-resolution bathymetry as roughly circular features; in our case >5 m high. Each was characterized by a circle approximating the base and a point representing its peak. Heights were measured relative to the average

*E-mail: i.a.yeo@durham.ac.uk.

[1]GSA Data Repository item 2012005, TOBI sidescan, SM2000 high-resolution bathymetry, and geological interpretation for area 2; high-resolution area 1 map; and statistics for identified hummocks in areas 1 and 2, is available online at www.geosociety.org/pubs/ft2012.htm, or on request from editing@geosociety.org or Documents Secretary, GSA, P.O. Box 9140, Boulder, CO 80301, USA.

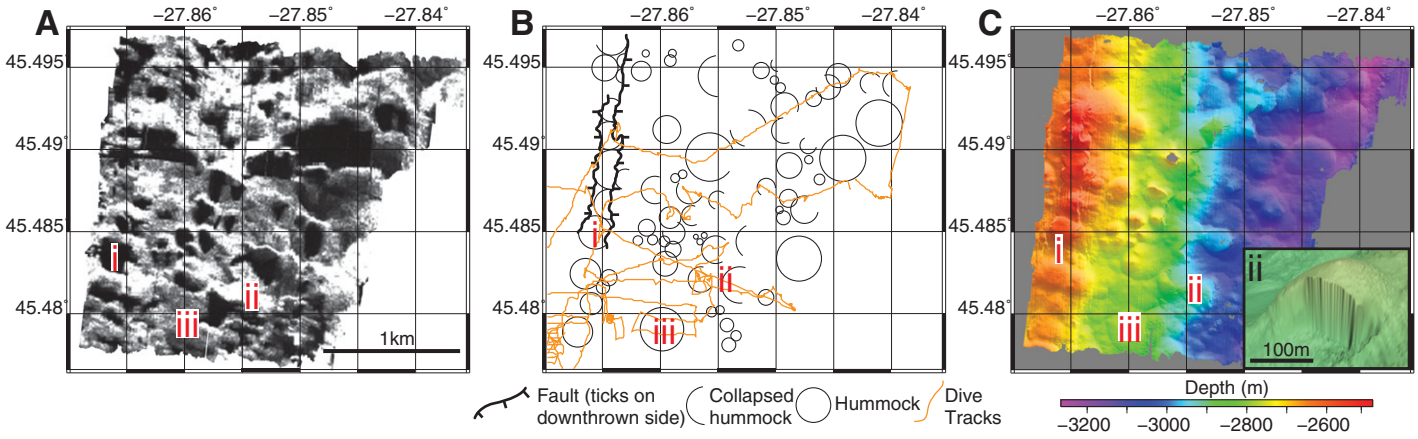

Figure 2. Data from area 1, in the North Atlantic Ocean. A: TOBI sidescan sonar mosaic of two south-looking images, joined near 45.49°N; the northern one overlapping the nadir of the southern. High backscatter is represented by light tones. B: Interpretation (only hummocks robust in both the sidescan sonar and SM2000 bathymetry are included). Three hummocks directly west of roman numerals i–iii are examples illustrated in Figure 4. High-resolution bathymetry allows for identification of features such as faults; hummock-limited collapses that are unresolved by TOBI. C: Corresponding area of high-resolution SM2000 bathymetry. Inset shows a three-dimensional visualization of the collapsed hummock (ii), viewed from the north, with no vertical exaggeration.

depth of the basal circle. Average flank slopes were calculated for each hummock, omitting areas of slumping, as $\tan^{-1}$ (height/radius) (see Table DR1 in the Data Repository for data).

Using this classification, area 1 contains 75 hummocks and area 2 contains 78, equivalent to 17 and 16 hummocks per km^2, respectively. Hummock heights range from 5 to 150 m and diameters from 30 to 330 m (Fig. 3A). Flank slopes range from 7º to 60º, with a mean of 27º. Height:diameter ratios show a large degree of scatter and are up to a factor of five greater than the typical 1:10 trend of seamounts (Smith et al., 1995a, 1995b).

The high-resolution bathymetry allows for the correlation of observed lava morphologies with specific areas (Fig. 4). Hummock flanks are built predominantly of pillows (Fig. 4A), which become elongate on steeper slopes (Fig. 4E). Hummock summits may be gently domed with lobate flows (Fig. 4H), or remain steep with round or elongate pillows (Fig. 4E). Summits often contain small haystacks (Stakes et al., 2006) 2–10 m high (Fig. 4F), which define the eruption focus. Small fissures are sometimes visible cutting hummocks (Fig. 4B).

Several clear fault scarps are visible, continuous over hundreds of meters, with throws up to 40 m (Fig. 2B; Fig. DR1 in the Data Repository). All are vertical or near-vertical and have associated talus deposits, identified from ROV *Isis* video and high-resolution bathymetry as smooth, fan-shaped deposits. Approximately 30% of hummocks are cut by subvertical scarps, which do not extend beyond the base of the hummock and are not associated with regional faulting (Fig. 2C, inset). These scarps produce near-vertical cliffs 5–150 m high that crosscut the hummocks and produce talus deposits at their bases. We interpret these as flank collapse scars. Both fault scarps (Fig. 4C) and collapse scarps (Fig. 4G) are composed of near-vertical walls of broken pillows with talus deposits (Fig. 4D).

DISCUSSION

Building Hummocks

It is generally agreed that lava morphology is controlled by effusion rate (Bonatti and Harrison, 1988; Fundis et al., 2010), and wax analogue experiments can provide approximate estimates of effusion rate (Gregg and Fink, 1995). Such experiments suggest that lavas with a viscosity of 100 Pa s (Dietrich et al., 1980) produce pillowed flows at low effusion rates (<1 m^3 s^{-1}), progressing to lobate (1–100 m^3 s^{-1}) and sheet flows (>100 m^3 s^{-1}) (Gregg and Fink, 1995; Gregg and Smith, 2003). While these experiments were conducted on 10° slopes (lower than the average slope in our study area), gravitational forces are not expected to exert control on morphology until slopes exceed 25° (Gregg and Smith, 2003) and do not dominate until 40° (Gregg and Fink, 1995), which is appropriate for 97% of observed hummocks.

We estimate hummock growth rates in area 1 using lava morphologies from summits (to minimize the effects of cooling). Twenty-four hummocks were imaged by ROV *Isis*, ten of which have lobate morphology. All have volumes <2.2 × 10^6 m^3 and would have formed in 0.1–25 days (using the upper limit of 100 m^3 s^{-1} and lower limit of 1 m^3 s^{-1}). Fourteen hummocks had pillowed morphology; the largest of these, with a volume of 4.1 × 10^6 m^3, would have taken >47 days of constant effusion to form, assuming an upper effusion rate limit of 1 m^3 s^{-1} (Griffiths and Fink, 1992). The remaining pillowed hummocks have volumes <1 × 10^6 m^3, and would have formed in >11 days at constant effusion.

No discernible sediment intercalations are seen in the collapsed cross sections of any hummocks, although we know our methods could detect them because sediment layers were seen in dives on the median valley wall faults. With a regional sedimentation rate of ~5 cm/k.y. (Keen and Manchester, 1970), we can thus rule out periods of quiescence on the thousand-year time scale. While continuous hummock effusion on the scale of days to years is difficult to prove, a single eruption origin seems likely. If we make the reasonable assumption that an average-sized hummock conduit is no more than 20 m wide, it would cool in ~13 yr or less (Turcotte and Schubert, 1982), so repeat eruptions would have to occur on this time scale if they are to exploit earlier thermally weakened zones. Thus, we suggest hummocks are monogenetic. It is possible the same fissure may erupt repeatedly, although we see no evidence of this.

We do not observe hummocks as eruptive lobes of larger, complex hummocky seamounts (e.g., Cann and Smith, 2005; Smith et al., 1995a), perhaps because such seamounts are more common at different stages in AVR evolution. However, we do see alignments of hummocks, both parallel and roughly orthogonal to the ridge axis (Searle et al., 2010, their figure 7), and suggest the AVR is largely composed of these alignments, produced during fissure eruptions (Head et al., 1996; Wylie et al., 1999). The ridge-parallel alignments (e.g., crest of AVR in Fig. 2) are typical of linear, fissure-fed eruptions of multiple hummocks (Smith and Cann, 1999), while the orthogonal spurs (e.g., WNW-ESE alignment from 27.856°W, 45.489°N) are aligned down the steepest parts of the AVR flanks and are probably gravity controlled (Searle et al., 2010). In

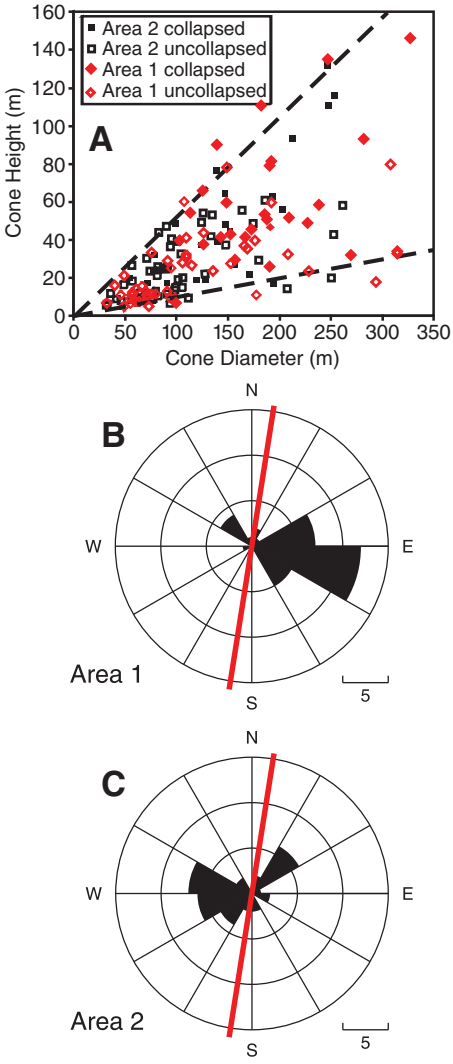

Figure 3. A. Height:diameter for hummocks identified in area 1 (red diamonds) and area 2 (black squares) in the North Atlantic Ocean. Collapsed hummocks are shown by filled symbols, uncollapsed hummocks by open symbols. Lower dashed line indicates 1:10 height:diameter ratio of flat-topped or hummocky seamounts; upper dashed line brackets the data with an upper height:diameter ratio of 1:2. B: Orientations of collapse directions for the 24 collapsed hummocks in area 1. Collapse direction vectors are normal to the scarp orientation. C: Orientations of collapse directions for the 28 collapsed hummocks in area 2.

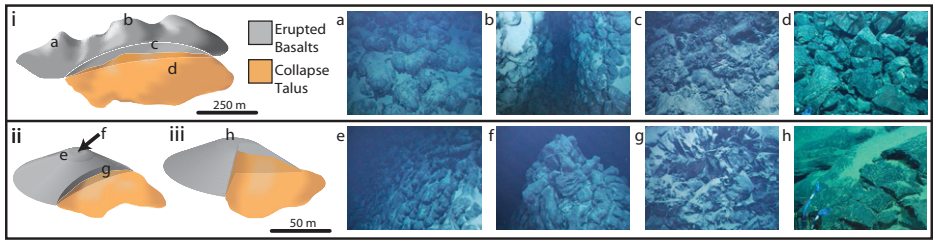

Figure 4. Left: Schematic diagrams of (i) faulted crest of the axial volcanic ridge (AVR), and (ii, iii) hummock-limited collapse structures (i, ii, iii correspond to Fig. 2). Right: Photos show typical morphologies observed in ROV *Isis* dives for different edifices and areas. Field of view between 1 m and 3 m. A: Pillows from a hummock flank (27°50′26.10W, 45°36′28.31N). B: Small open fissure on a hummock summit (27°52′16.16W, 45°28′56.26N). C: Near-vertical face of a fault scarp showing truncated pillows (27°50′26.52W, 45°29′13.21N). D: Talus at base of a scarp (27°51′44.28W, 45°29′24.32N). E: Steeply draped elongate pillows near a hummock summit (27°53′21.12W, 45°23′42.75N). F: Small haystack at a steep hummock summit (27°52′32.17W, 45°24′1.81N). G: Truncated pillows in the vertical wall of a collapse scar (27°47′8.82W, 45°42′17.76N). H: Gently domed hummock summit characterized by lightly sedimented lobate lavas (27°50′59.45W, 45°29′31.18N).

both cases, a single eruption builds a number of hummocks.

Timing and Melt Fluxes

The AVR volume is ~16 km^3, assuming a flat base at ~3100 m. It sits within an axial valley 6 km wide at its center, representing 286 ka at the full spreading rate of 2.1 cm yr^{-1}; the maximum possible AVR age. This yields a minimum magma flux to the seafloor of 5.6 × 10^4 m^3 yr^{-1}, sufficient to produce one average hummock every 5 yr. AVR lineaments comprise an average of 12 hummocks (Searle et al., 2010), so assuming each lineament represents a single fissure eruption (Smith and Cann, 1999) and assuming the whole AVR is built only by such eruptions, they would occur approximately every 60 yr and have average volumes of ~3.5 × 10^6 m^3. This is similar to eruption volumes on the fast-spreading East Pacific Rise, and differs from estimates suggesting eruption volumes should be significantly larger at slow-spreading ridges (Perfit and Chadwick, 1998; Sinton et al., 2002; Soule et al., 2007).

Alternatively, assuming the AVR is built entirely of average-sized (2.95 × 10^5 m^3) hummocks, it would contain ~55,000 hummocks. With our observed ratio of 42% lobate and 58% pillowed hummocks and the effusion rates estimated above, the entire AVR could be built in only 300 yr, or less if hummocks are erupted in groups. This is much lower than other published estimates (e.g., Searle et al., 2010) and implies lower effusion rates and/or large eruptive pauses

Hummock Collapse

One third of the hummocks in area 1 and 25% of those in area 2 have suffered collapse (Fig. 2 inset, and Fig. 3). Figures 3B and 3C show two prominent alignments in the strikes of collapse normals at ~095° and 275°, approximately normal to the strike of the ridge axis.

There is no evidence of a collapse threshold for hummocks in either height, diameter, or height:diameter ratio, arguing against simple slope instability as a cause. However, most collapse directions are normal to the local seafloor slope, suggesting that collapses are gravity driven. Collapsing hummocks within volcanic alignments may also be buttressed by flanking edifices, allowing them to collapse only on their free edges (Hammond, 1997), which are, for the most part, parallel to the AVR axis.

Seismic Layer 2A

Flank collapse is clearly very common and a fundamental process in the development of this volcanic terrain that eventually forms the upper oceanic crust.

In our study areas, ~ 33% of hummocks have collapsed, with each collapsed hummock losing ~40% of its volume. Thus, ~12% of all lavas that erupted as hummocks (essentially 12% of the AVR) end up as talus. The porosity of pillow lava systems is 0.3% to 11.3% (Goldberg et al., 2008; Johnson and Christensen, 1997), with a mean of 3.4% (Johnson and Christensen, 1997) for intact basalts and ~20% for fractured basalts (Goldberg et al., 2008). Talus deposits have much greater porosities, perhaps >40% (Freeze and Cherry, 1979), thus a young buried talus flow could significantly increase the effective porosity in the crust. The addition of 12% of such material could increase the average upper crustal porosity by 3.4%–4.8% compared to unfractured pillowed crust, and by 2.4% compared to fractured pillowed crust. Wilkens et al. (1991) showed that an increase in porosity of ~3% can reduce seismic velocity by >0.5 km/s, so this could make a substantial contribution to velocity reduction in upper oceanic crust.

Goldberg and Sun (1997) note that drill logs from slow-spreading crust show higher porosity than those from intermediate-spreading ridges, yet seismic layer 2A velocities at most spreading rates are between 2 and 5 km/s (Barclay and Wilcock, 2004; Grevemeyer et al., 1998; Hussenoeder et al., 2002a, 2002b; Jacobs et al., 2007) and show no consistent pattern of higher porosities at slow-spreading ridges. However, fast-spreading ridges have more drained sheet flows and lava tubes, both of which are major contributors to porosity. Thus, the large talus component being added to the crust may be the dominant mechanism for lowering the effective porosity of the upper oceanic crust at slow-spreading ridges.

CONCLUSIONS

Volcanic hummocks observed in sidescan images are confirmed to be small, probably monogenetic, cones and domes, with flanks formed predominantly of pillow lavas and summits of pillow or lobate flows. The estimated melt flux to the seafloor is sufficient to produce average-sized eruptions feeding, on average, 12 hummocks approximately every 60 yr. Up to 33% of AVR hummocks have collapsed, mostly along the local topographic gradient. The associated talus deposits may be a significant cause of reduced upper-oceanic-crust seismic velocity at slow-spreading ridges, where lower average eruption rates inhibit the formation of macroscopic pore spaces characteristic of faster-spreading ridges.

ACKNOWLEDGMENTS

This work was funded by the Natural Environment Research Council (NERC). Yeo acknowledges receipt of an NERC postgraduate studentship. We thank the shipboard scientific party, officers, crew, and technicians of RRS *James Cook* cruise 24 for their dedication and professionalism in assisting in the data acquisition. We also thank John Maclennan, Joe Cann, Suzanne Carbotte, and an anonymous reviewer for their careful reviews, which have greatly improved the manuscript.

REFERENCES CITED

Ballard, R.D., and Moore, J.G., 1977, Photographic Atlas of the Mid-Atlantic Ridge Rift Valley: New York, Springer-Verlag, 114 p.

Barclay, A.H., and Wilcock, W.S.D., 2004, Upper crustal seismic velocity structure and microearthquake depths at the Endeavour Segment, Juan de Fuca Ridge: Geochemistry Geophysics Geosystems, v. 5, Q01004, doi:10.1029/2003GC000604, doi:10.1029/2003GC000604.

Bonatti, E., and Harrison, C.G.A., 1988, Eruption styles of basalts in oceanic spreading ridges and seamounts—Effect of magma temperature and viscosity: Journal of Geophysical Research, v. 93, p. 2967–2980, doi:10.1029/JB093iB04p02967.

Cann, J.R., and Smith, D.K., 2005, Evolution of volcanism and faulting in a segment of the Mid-Atlantic Ridge at 25 degrees N: Geochemistry Geophysics Geosystems, v. 6, p. 1–20, doi:10.1029/2005GC000954.

Dietrich, G.K., Krauss, K.W., and Siedler, G., 1980, General Oceanography: New York, John Wiley, 625 p.

Flewellen, C., Millard, N., and Rouse, I., 1993, TOBI, A vehicle for deep ocean survey: Electronics & Communication Engineering Journal, v. 5, p. 85–93, doi:10.1049/ecej:19930015.

Freeze, R.A., and Cherry, J.A., 1979, Groundwater: Hemel Hempstead, UK, Prentice Hall, 604 p.

Fundis, A.T., Soule, S.A., Fornari, D.J., and Perfit, M.R., 2010, Paving the seafloor: Volcanic emplacement processes during the 2005–2006 eruptions at the fast spreading East Pacific Rise, 9° 50' N: Geochemistry Geophysics Geosystems, v. 11, Q08024, doi:10.1029/2010GC003058.

German, C., Tyler, P., and Griffiths, G., 2003, The maiden voyage of UK ROV "Isis": Ocean Challenge, v. 12, p. 16–18.

Goldberg, D., and Sun, Y.F., 1997, Attenuation differences in layer 2A in intermediate- and slow-spreading oceanic crust: Earth and Planetary Science Letters, v. 150, p. 221–231, doi:10.1016/S0012-821X(97)00097-6.

Goldberg, D.S., Takahashi, T., and Slagle, A.L., 2008, Carbon dioxide sequestration in deep-sea basalt: Proceedings of the National Academy of Sciences of the United States of America, v. 105, p. 9920–9925, doi:10.1073/pnas.0804397105.

Gregg, T.K.P., and Fink, J.H., 1995, Quantification of submarine lava-flow morphology through analog experiments: Geology, v. 23, p. 73–76, doi:10.1130/0091-7613(1995)023<0073:QOSLFM>2.3.CO;2.

Gregg, T.K.P., and Smith, D.K., 2003, Volcanic investigations of the Puna Ridge, Hawai'i: relations of lava flow morphologies and underlying slopes: Journal of Volcanology and Geothermal Research, v. 126, p. 63–77, doi:10.1016/S0377-0273(03)00116-1.

Grevemeyer, I., Weigel, W., and Jennrich, C., 1998, Structure and ageing of oceanic crust at 14°S on the East Pacific Rise: Geophysical Journal International, v. 135, p. 573–584, doi:10.1046/j.1365-246X.1998.00673.x.

Griffiths, R.W., and Fink, J.H., 1992, Solidification and morpholoy of submarine lavas—A dependence on extrusion rate: Journal of Geophysical Research, v. 97, p. 19729–19737, doi:10.1029/92JB01594.

Hammond, S.R., 1997, Offset caldera and crater collapse on Juan de Fuca ridge-flank volcanoes: Bulletin of Volcanology, v. 58, p. 617–627, doi:10.1007/s004450050166.

Head, J.W., Wilson, L., and Smith, D.K., 1996, Mid-ocean ridge eruptive vent morphology and substructure: Evidence for dike widths, eruption rates, and evolution of eruptions and axial volcanic ridges: Journal of Geophysical Research, v. 101, p. 28265–28280, doi:10.1029/96JB02275.

Hussenoeder, S.A., Detrick, R.S., Kent, G.M., Schouten, H., and Harding, A.J., 2002a, Fine-scale seismic structure of young upper crust at 17°20'S on the fast spreading East Pacific Rise: Journal of Geophysical Research, v. 107, 2158, doi:10.1029/2001JB001688.

Hussenoeder, S.A., Kent, G.M., and Detrick, R.S., 2002b, Upper crustal seismic structure of the slow spreading Mid-Atlantic Ridge, 35°N: Constraints on volcanic emplacement processes: Journal of Geophysical Research, v. 107, 2156, doi:10.1029/2001JB001691.

Jacobs, A.M., Harding, A.J., and Kent, G.M., 2007, Axial crustal structure of the Lau back-arc basin from velocity modeling of multichannel seismic data: Earth and Planetary Science Letters, v. 259, p. 239–255, doi:10.1016/j.epsl.2007.04.021.

Johnson, J.E., and Christensen, N.I., 1997, Seismic properties of layer 2 basalts: Geophysical Journal International, v. 128, p. 285–300, doi:10.1111/j.1365-246X.1997.tb01555.x.

Keen, M.J., and Manchester, K.S., 1970, The Mid-Atlantic Ridge near 45ºN. X. Sediment distribution and thickness from seismic reflection profiling: Canadian Journal of Earth Sciences, v. 7, p. 735–747, doi:10.1139/e70-075.

LeBas, T.P., and Huvenne, V.A.I., 2009, Acquisition and processing of backscatter data for habitat mapping—Comparison of multi-beam and side-scan systems: Applied Acoustics, v. 70, p. 1248–1257.

Perfit, M.R., and Chadwick, W., 1998, Magmatism at mid-ocean ridges: Constraints from volcanological and geochemical investigations, *in* Buck, R., ed., Faulting and magmatism at mid-ocean ridges: American Geophysical Union Geophysical Monograph 106, p. 59–116.

Searle, R.C., and 13 others, 2010, Structure and development of an axial volcanic ridge: Mid-Atlantic Ridge, 45°N: Earth and Planetary Science Letters, v. 299, p. 228–241, doi:10.1016/j.epsl.2010.09.003.

Sinton, J., Bergmanis, E., Rubin, K., Batiza, R., Gregg, T.K.P., Gronvold, K., Macdonald, K.C., and White, S.M., 2002, Volcanic eruptions on mid-ocean ridges: New evidence from the superfast spreading East Pacific Rise, 17°–19°S: Journal of Geophysical Research, v. 107, p. 2115–2134, doi:10.1029/2000JB000090.

Smith, D.K., and Cann, J.R., 1990, Hundreds of small volcanoes on the median valley floor of the Mid-Atlantic Ridge at 24°–30°N: Nature, v. 348, p. 152–155, doi:10.1038/348152a0.

Smith, D.K., and Cann, J.R., 1992, The role of seamount volcanism in crustal construction and the Mid-Atlantic Ridge (24°–30°N): Journal of Geophysical Research, v. 97, p. 1645–1658, doi:10.1029/91JB02507.

Smith, D.K., and Cann, J.R., 1993, Building the crust at the Mid-Atlantic Ridge: Nature, v. 365, p. 707–715, doi:10.1038/365707a0.

Smith, D.K., and Cann, J.R., 1999, Constructing the upper crust of the Mid-Atlantic Ridge: A reinterpretation based on the Puna Ridge, Kilauea Volcano: Journal of Geophysical Research, v. 104, p. 25379–25399, doi:10.1029/1999JB900177.

Smith, D.K., Cann, J.R., Dougherty, M.E., Lin, J., Spencer, S., MacLeod, C., Keeton, J., McAllister, E., Borroks, B., Pascoe, R., and Robertson, W., 1995a, Mid-Atlantic Ridge volcanism from deep-towed side-scan sonar images, 25°–29°N: Journal of Volcanology and Geothermal Research, v. 67, p. 233–262, doi:10.1016/0377-0273(94)00086-V.

Smith, D.K., Humphris, S.E., and Bryan, W.B., 1995b, A comparison of volcanic edifices at the Reykjanes Ridge and the Mid-Atlantic Ridge at 24°–30°N: Journal of Geophysical Research, v. 100, p. 22485–22498, doi:10.1029/95JB02392.

Smith, D.K., Tivey, M.A., Gregg, P.M., and Kong, L.S.L., 2001, Magnetic anomalies at the Puna Ridge, a submarine extension of Kilauea Volcano: Implications for lava deposition: Journal of Geophysical Research, v. 106, p. 16,047–16,060, doi:10.1029/2000JB000014.

Soule, S.A., Fornari, D.J., Perfit, M.R., and Rubin, K.H., 2007, New insights into mid-ocean ridge volcanic processes from the 2005–2006 eruption of the East Pacific Rise, 9°46'N–9°56'N: Geology, v. 35, p. 1079–1082, doi:10.1130/G23924A.1.

Stakes, D.S., Perfit, M.R., Tivey, M.A., Caress, D.W., Ramirez, T.M., and Maher, N., 2006, The Cleft revealed: Geologic, magnetic, and morphologic evidence for construction of upper oceanic crust along the southern Juan de Fuca Ridge: Geochemistry Geophysics Geosystems, v. 7, Q04003, doi:10.1029/2005GC001038.

Turcotte, D.L., and Schubert, G., 1982, Geodynamics applications of continuum physics to geological problems: New York, Wiley, 456 p.

Wilkens, R.H., Fryer, G.J., and Karsten, J., 1991, Evolution of porosity and seismic structure of upper oceanic-crust—Importance of aspect ratios: Journal of Geophysical Research, v. 96, p. 17981–17995, doi:10.1029/91JB01454.

Wylie, J.J., Helfrich, K.R., Dade, B., Lister, J.R., and Salzig, J.F., 1999, Flow localization in fissure eruptions: Bulletin of Volcanology, v. 60, p. 432 440, doi:10.1007/s004450050243.

Manuscript received 27 October 2010
Revised manuscript received 25 August 2011
Manuscript accepted 2 September 2011

Printed in USA